High-Voltage, High-Impedance Ion Beam Production*

David Hinshelwood, S.L. Jackson, R.J. Allen, R.J. Commisso, G. Cooperstein, D. Mosher,[a] D.P. Murphy, P.F. Ottinger, J.W. Schumer, S.B. Swanekamp,[a] B.V. Weber, and F.C. Young[a]

Plasma Physics Division
Naval Research Laboratory
Washington, DC 20375 USA

Abstract

A high-power, high-impedance ion beam diode has been fielded on the Mercury inductive voltage adder at typical parameters of 4 MV, 360 kA, and 70-90-kA ion current. These results are consistent with theory and with LSP calculations. This beam is focused onto a CF_2 target to produce characteristic gammas via the $^{19}F(p,\alpha\gamma)^{16}O$ reaction. Diagnostics characterize the ion emission from the anode, the beam distribution on the target, and the gamma yield. Shaping the anode surface improves beam focusing on the target. Our experimental arrangement allows us to resolve the gamma signal in the presence of the diode bremsstrahlung, and to minimize spurious neutron production. The calculated gamma yield exceeds 10^{11} gammas/sr.

I. INTRODUCTION

We are investigating the use of TW-level pulsed power in inducing fission in fissionable material. This is directed toward the detection of smuggled illicit material [1]. Different sources are considered:

1. Characteristic gammas from the $^{19}F(p,\alpha\gamma)^{16}O$ reaction [2].
2. 7-15-MV-endpoint thin-target bremsstrahlung.
3. Neutrons from ion-beam-target reactions

Modeling indicates that intense pulsed sources offer desirable advantages in certain operational scenarios.

We have begun by studying the first approach, because of its potential for reducing collateral dose, and its synergy with the third approach (with an appropriate target, ion beams can generate combinations of characteristic gammas and neutrons). The characteristic-gamma yield as a function of proton voltage [2] is shown in Fig. 1. The yield reaches a maximum at about 4 MV.

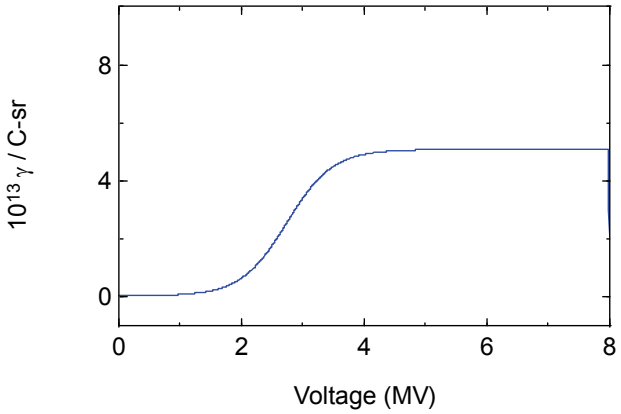

Figure 1. Characteristic-gamma yield for protons on fluorine via $^{19}F(p,\alpha\gamma)^{16}O$, from Ref. 2

This paper describes ion-beam diode experiments on the Mercury inductive voltage adder at ~4-MV, ~360-kA total current, and 70-90-kA ion current. Conversion of Mercury to positive polarity, accompanied by extensive circuit-code and P-I-C-code modeling, is described in Refs. 3 and 4.

Inductive-voltage-adder operation has a significant dependence on polarity. In negative polarity, all electrons are born at the same potential, and the magnetically-insulated-transmission-line [MITL] flow can be well characterized. In positive polarity, electrons emitted from each section are born at different potentials. This causes the electron flow current to be larger and more distributed over the gap, as shown in Fig. 2. This has two consequences for diode operation: First, optimum coupling to the generator occurs at lower impedance. For Mercury the optimum coupling occurs at 20-24 Ohms for negative and 10-12 Ohms for positive polarity. Second, the nature of the flow precludes determination of the diode voltage, as will be discussed in Sec. III. The work described in this paper follows extensive modeling of Mercury operation in positive polarity [4].

* Work supported by the US Office of Naval Research
ξ email: ddh@suzie.nrl.navy.mil
[a] L3 Communications, Inc, Reston, VA.

Report Documentation Page

Form Approved
OMB No. 0704-0188

1. REPORT DATE	2. REPORT TYPE	3. DATES COVERED
JUN 2009	**N/A**	**-**

4. TITLE AND SUBTITLE	5a. CONTRACT NUMBER
High-Voltage, High-Impedance Ion Beam Production	5b. GRANT NUMBER
	5c. PROGRAM ELEMENT NUMBER
6. AUTHOR(S)	5d. PROJECT NUMBER
	5e. TASK NUMBER
	5f. WORK UNIT NUMBER
7. PERFORMING ORGANIZATION NAME(S) AND ADDRESS(ES) **Plasma Physics Division Naval Research Laboratory Washington, DC 20375 USA**	8. PERFORMING ORGANIZATION REPORT NUMBER
9. SPONSORING/MONITORING AGENCY NAME(S) AND ADDRESS(ES)	10. SPONSOR/MONITOR'S ACRONYM(S)
	11. SPONSOR/MONITOR'S REPORT NUMBER(S)

12. DISTRIBUTION/AVAILABILITY STATEMENT
Approved for public release, distribution unlimited

13. SUPPLEMENTARY NOTES
See also ADM002371. 2013 IEEE Pulsed Power Conference, Digest of Technical Papers 1976-2013, and Abstracts of the 2013 IEEE International Conference on Plasma Science. IEEE International Pulsed Power Conference (19th). Held in San Francisco, CA on 16-21 June 2013., The original document contains color images.

14. ABSTRACT
high-power, high-impedance ion beam diode has been fielded on the Mercury inductive voltage adder at typical parameters of 4 MV, 360 kA, and 70-90-kA ion current. These results are consistent with theory and with LSP calculations. This beam is focused onto a CF2 target to produce characteristic gammas via the 19F(p,áã)16O reaction. Diagnostics characterize the ion emission from the anode, the beam distribution on the target, and the gamma yield. Shaping the anode surface improves beam focusing on the target. Our experimental arrangement allows us to resolve the gamma signal in the presence of the diode bremsstrahlung, and to minimize spurious neutron production. The calculated gamma yield exceeds 1011 gammas/sr.

15. SUBJECT TERMS

16. SECURITY CLASSIFICATION OF:			17. LIMITATION OF ABSTRACT	18. NUMBER OF PAGES	19a. NAME OF RESPONSIBLE PERSON
a. REPORT	b. ABSTRACT	c. THIS PAGE			
unclassified	**unclassified**	**unclassified**	**SAR**	**6**	

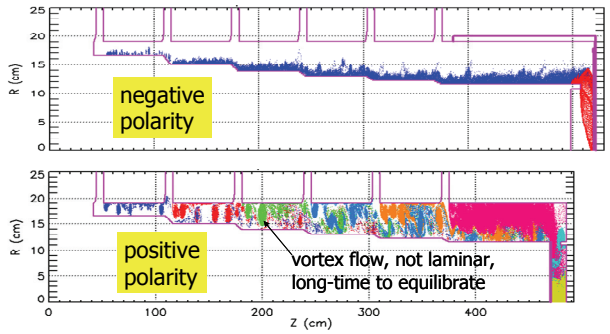

Figure 2: Results of LSP [5] simulations of inductive voltage adders, from Ref. 4.

High-power ion beam generation was studied extensively at NRL and elsewhere in the last century. Most of this work, however, involved operation below 5 Ohms. The ion efficiency (fraction of the total current) in a pinched-beam diode scales inversely with the diode impedance [6], so that a reduced ion efficiency will be expected at the 10-12-Ohm diode impedance in this current work. Higher-impedance pinched-beam ion-diode operation was studied in the past [7], where ~20% ion efficiency was obtained. This work parallels ongoing experiments at Sandia National Labs [8].

The 4-MV Mercury operating point is well suited to this application: achieving the peak gamma yield while avoiding unwanted beam-target nuclear reactions at higher ion energies.

II. EXPERIMENTAL ARRANGEMENT

The diode region is shown in Fig. 3. Design of the ion diode is driven by the need to shield the diagnostics from the 4-MV-end-point diode bremsstrahlung that will greatly exceed the gamma yield. We use a 1-meter-OD, 10-cm-ID, 15-cm-thick lead annulus to accomplish this. The ion beam is injected through the shield via a 9-cm-ID aluminum tube and impinges on the target located near the back end of the lead. Diagnostics viewing the target from locations off the axis are thus shielded from diode radiation. This arrangement in turn dictates a small diode diameter and an anode axial location as close as possible to the disk. The anode foil, typically 0.25-mm-thick PVA, is mounted at the end of a 6.1-cm-diam, 17-cm-long section of aluminum tube that extends from the end of the MITL.

The circles in Fig. 3 indicate the locations of current monitors employed here. The diode is separated from the last IVA cell by ~1 meter of constant-impedance MITL. Inner and outer monitors (red and magenta) are located just beyond the last IVA cell, about 1 meter upstream from the diode. The outer current at the load (cyan) is measured opposite the anode extension. The inner current at the load is measured at two locations: 20-cm upstream (blue) and at the front face of the MITL (green). The ion current is measured behind the cathode.

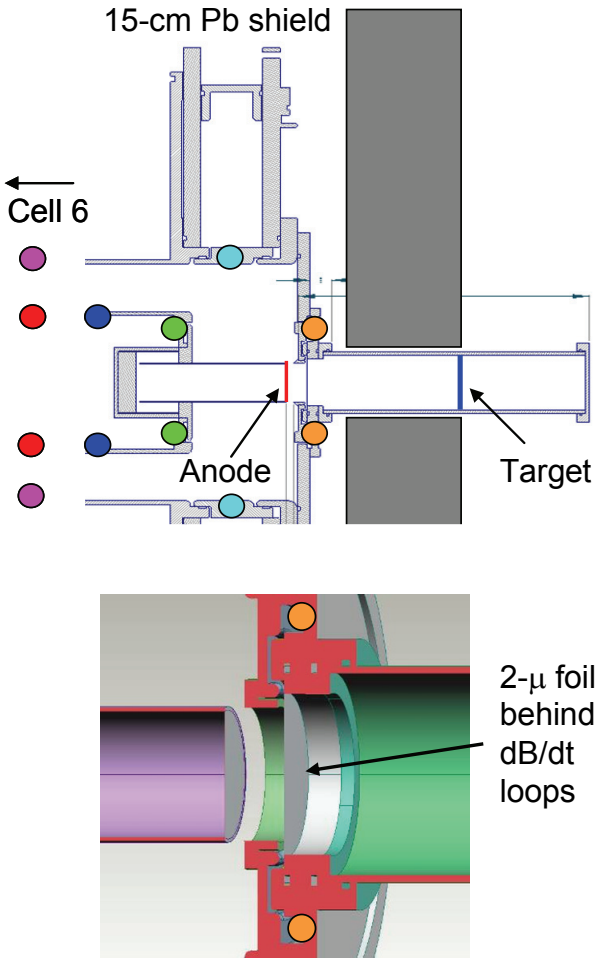

Figure 3. (top) The Mercury ion diode, showing locations of current monitors; (bottom) details of the ion current monitor.

Details of the ion current monitor are also shown in Fig. 3. A thin foil is located just behind the slot containing the dB/dt loops. Both previous experience and LSP [5] modeling indicate that this foil should be recessed behind the cathode tip by about 1-2 A-K-gap lengths. This is deep enough to prevent electron emission from the foil (which would overstate the ion current) while avoiding virtual anode formation and consequent electron current to the foil (which would understate the ion current).

Typical current signals are shown in Fig. 4. The trace colors correspond to the circles in Fig. 3. Upstream of the diode, the vacuum flow is about 25% of the total current (red and magenta curves). This is virtually unchanged up to the diode location (blue and cyan). The outer (cathode) current monitors (magenta and cyan) show the expected propagation of the retrapping wave back from the diode from 30-50 ns. There is a small current loss at the transition to the small anode tube (blue and green). The ion current efficiency is about 25%. All of this is in good agreement with LSP modeling and with analytic theory.

Modeling also predicts little additional loss between the base of the tube (green) and the diode. The crowbarring of the ion current is attributed to shorting of the ion db/dt-loop-slot by plasma expanding from the foil.

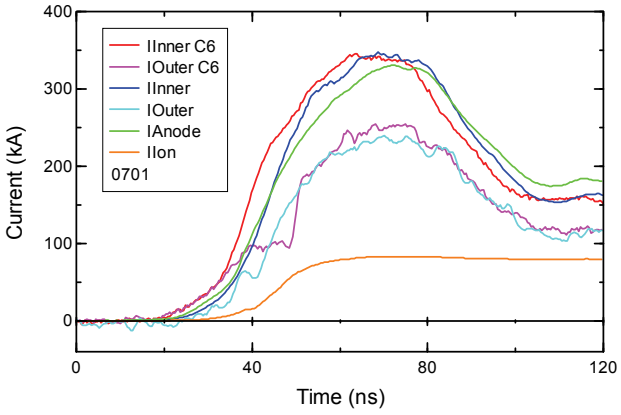

Figure 4. Typical current waveforms. The colors match the circles in Fig. 3.

III. DIODE VOLTAGE

The presence of flow electrons in MITL's precludes direct measurement of the voltage. MITL flow theory originated by Mendel [4, 9] relates the voltage to the anode and cathode currents, in a line with equilibrium flow. This theory is now fairly mature and has demonstrated success in determining the voltage in negative-polarity adders where all electrons are born at the same potential. But there is as yet no satisfactory theory that allows calculation of voltage in a positive-polarity-adder MITL. In principle, measurement of the diode current can be used to determine the voltage. Ion-diode theory [6] predicts that the impedance and ion efficiency of a pinched-beam ion diode are given by

$$V = -\frac{mc^2}{e} + \left[\left(\frac{mc^2}{e}\right)^2 + \left(\frac{\alpha D I_a}{R}\right)^2\right]^{1/2} \quad \text{and}$$

$$\frac{I_i}{I_e} = \left(\frac{2m_e}{m_i}\right)^{1/2} (1+\gamma)^{1/2} \frac{R}{D}$$

where ***R*** is the diode radius, ***D*** is the gap, and α is a scaling factor.

In practice, we need to know the appropriate values for α and how to define the current in the above equations in the case where there is significant vacuum flow. A series of simulations using LSP [4] indicate that these formulae give an accurate description of the diode when α is set to 36 and the current is set to the full (vacuum + bound) current. Fig. 5 shows the voltage calculated using these equations and assuming an effective diode closure velocity of 2 cm/us. The voltage is calculated to peak at just under 4 MV, and the calculated ion current fits the measured value quite well until the monitors fail.

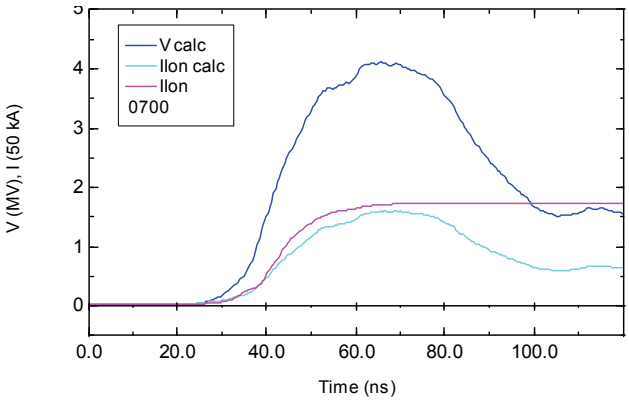

Figure 5. Calculated diode voltage (blue) and ion current (cyan) based on the measured total current.

The estimated voltage of ~4 MV is consistent with stacked-foil and activation data that will be discussed in Sec. 7.

IV. DIAGNOSTICS

Diagnostics employed in this work are shown in Fig. 6. For most shots a 0.25-mm-thick CF_2 disk served as the target. Characteristic-gamma radiation from this target was measured by a scintillator-photomultiplier combination shielded with several inches of lead. This radiation was also imaged using a 2-D tungsten rolled edge and radiographic image plate. A 1.6-mm-diam pinhole in 0.25-mm-thick aluminum, located behind a 3-mm-diam hole in the target, allowed a small portion of the beam to pass through to a 5-layer stack of FWT-60 radiachromic film [10] located 15 cm behind the target. This film stack images the anode foil and provides an estimate of the diode voltage.

V. GAMMA MEASUREMENT

A typical characteristic-gamma signal (blue) is shown in Fig. 7. The red trace shows the corresponding signal from a shot where the CF_2 was replaced by CH_2. Other than a very small initial spike that is attributed to bremsstrahlung, no signal is seen without the CF_2 target. Therefore we believe that we have a good measure of the gamma output. The green curve in the figure shows the yield (shown in arbitrary units) calculated based on the calculated ion voltage and current and the yield from Ref. 2. It agrees well in shape and timing with the measured signal. Based on this calculation, we would obtain a characteristic-gamma yield of 1.6×10^{11} gammas/sr if the entire beam strikes the target.

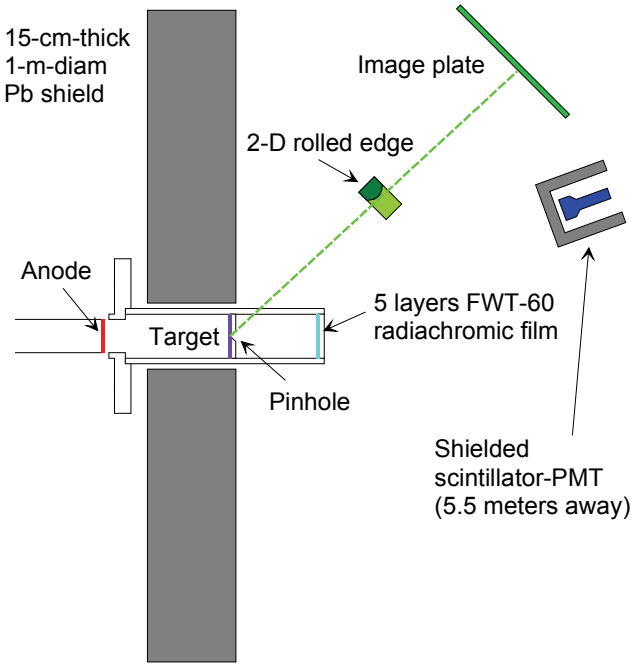

Figure 6. Diagnostics used in this experiment

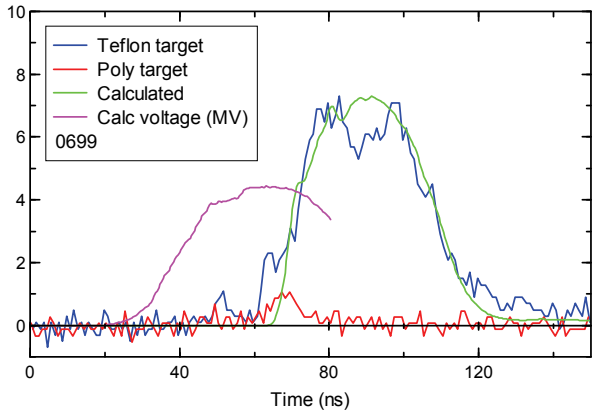

Figure 7. Gamma signals compared for shots with CF_2 (blue) and CH_2 (red) targets. The calculated signal is shown in arbitrary units in green.

The gamma detector also records a significant late-time neutron signal, as shown by the blue curve in Fig. 8. While mixed gamma-neutron output may be useful in some operational scenarios, the neutron signal is undesirable in this physics-based experiment. We find that it is dominated not by ion beam reactions at the target, but by ions moving backward into the anode tube. Electrons entering this tube form a virtual cathode that draws ions from the anode back into the tube, where they strike the rear of the can (see Fig. 3) with an energy that can exceed the diode voltage. Preventing the virtual cathode by placing a rigid backstop behind the anode foil caused unacceptable debris ejection back up the MITL. Instead, we fill the anode tube with a loosely-crumpled, thin aluminized-mylar foil. This spoils the virtual cathode and greatly reduces the neutron signal, as seen in the red curve in Fig. 8. This picture is consistent with observed damage to the diode hardware: without the foil, the anode tube was undamaged and material at the rear of the cup was blown away. With the foil, the sides of the anode tube had multiple holes blown out.

Interestingly, we see no difference in any other diagnostics when the virtual cathode (and thus electron reflexing) is prevented. Evidently, reflexing is not important to the diode operation under these conditions.

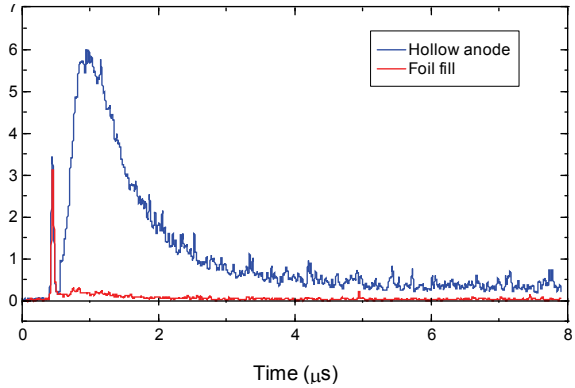

Figure 8. The gamma signal displayed on a longer timescale to show the late-time neutron contribution for shots without (blue) and with (red) virtual cathode suppression.

VI. TARGET IMAGING

The beam profile on the target is diagnosed by interposing a 2-D tungsten rolled edge between the source and a radiographic-image-plate detector. Each point on the image records radiation from a quarter plane at the source. A typical image is shown at the top of Fig. 9. Taking a line-out transverse to each edge and differentiating yields the line-spread functions, which represent the line integral of the beam profile along each edge direction. In principle, and assuming azimuthal symmetry, these could be Abel-inverted to yield the beam profile. Because of the noisy line spreads, however, we find it more useful to compare the line spreads directly with that calculated for a uniform disk distribution. This is shown in the bottom of Fig. 9. Within the resolution of this diagnostic, the beam appears close to uniform over the target, suggesting that much of the beam may be missing the target.

Calculation of ion magnetic bending in the diode predicts that the ions will over-focus, reaching the axis well before, and then spreading out at, the axial location of the target-plane. In an effort to correct for this, convex anode foils with 10-cm-radius were used. With these, the beam distribution on the target narrows and the gamma signal increases, as seen in Fig 10.

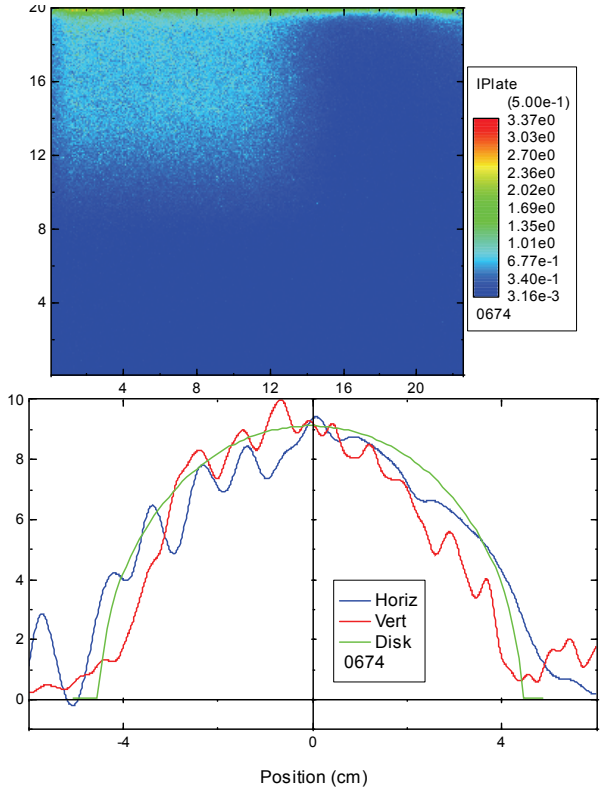

Figure 9. (top) Scanned image-plate exposure; (bottom) Horizontal and vertical line-spreads compared with that from a uniform disk (green).

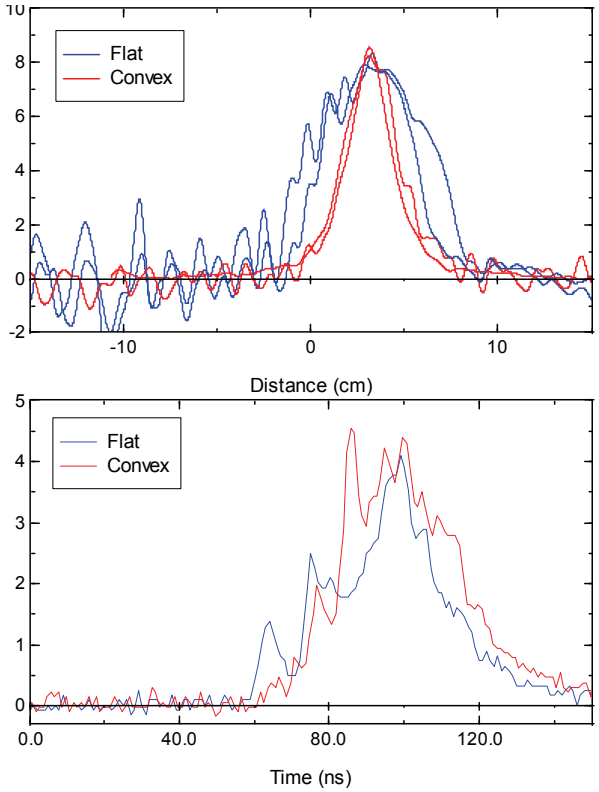

Figure 10. (top) line spreads for shots with flat (blue) and convex (red) anodes; (bottom) corresponding gamma signals.

VII. RADIACHROMIC FILM MEASUREMENTS

The pinhole at the center of the target conjugates the anode plane with the radiachromic film plane (see Fig. 6). If the ions follow ballistic (straight-line) trajectories in the drift tube (see Sec. VIII), then (except for the small displacement associated with bending in the diode) it is straightforward to map points on the film plane to the anode plane. The exposure at the film plane is then a measure of how many ions from the corresponding point on the anode reach the pinhole.

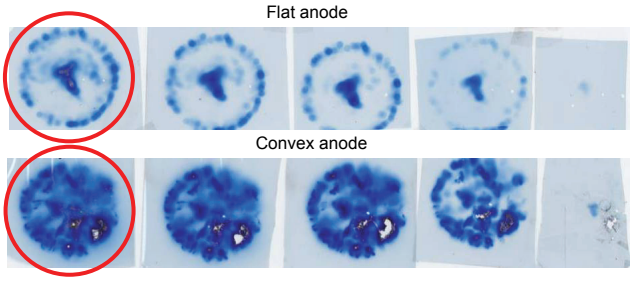

Figure 11. Exposed radiachromic films for shots with flat and convex anodes. The films are ordered left-to-right, with the top films at the left.

Films for flat and convex anodes are shown in Fig. 11. Each row shows the five films for that shot, with the front film at the left. The red circles indicate the diameter of the anode and cathode tip. For the flat anode, we observe a ring of exposure that is about 1 A-K gap in from the tip, and a more intense spot on axis. We tentatively identify the former with ions emitted before strong pinching has begun, when electron bending of this amount would be expected. The concentration of emission at the center arises from a combination of two factors: ion emission is strongest at the center, and ions emitted from off-axis locations over-focus and do not reach the pinhole. With the convex anode, we see substantial exposure at all radii, indicating that this shape allows a greater range of ions to reach the pinhole.

The relative exposure of films in the stack shows some shot-to-shot variation, but in general there is a very large fall-off from the fourth to the fifth film, with the latter having minimal exposure. Figure 12 shows calculated deposition profiles in this film assuming the calculated voltage and ion-current waveshapes in Fig. 5. These data indicate a peak voltage just over 4 MV.

This is consistent with our detection of ^{63}Zn activation on a few shots with copper targets. The ^{63}Cu(p,n)^{63}Zn reaction has a threshold of 4.15 MV.

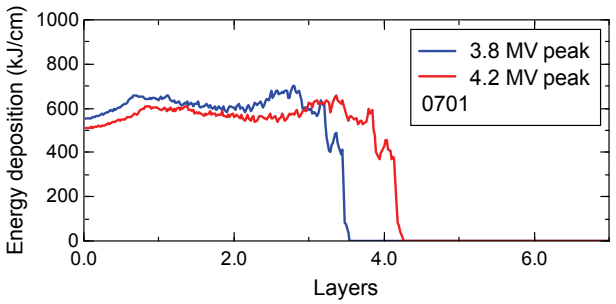

Figure 12. Calculated deposition profiles in the film stack for different peak voltages, using waveshapes in Fig. 5.

VIII. OTHER VARIATIONS

Most of these shots had a vacuum (< 20 mTorr) ambient in the drift tube. Based on our previous experience, we would expect charge, but not necessarily current, neutralization of the beam under these conditions. One shot was taken with the drift tube at a 1-Torr air ambient. This is approximately the optimum pressure for beam-induced ionization and so we would expect essentially complete charge and current neutralization on this shot. This shot showed no difference in gamma yield, beam profile on target, or radiachromic film image. From this we infer that even in vacuum the beam becomes well current-neutralized by electrons pulled off nearby surfaces. We attribute this to the relatively small diameter of the drift tube. This gives confidence to the assumption of ballistic trajectories used in analyzing the film images.

We also see no difference between anode surfaces of bare PVA, PVA coated with a thin layer of paraffin, or PVA sprayed with colloidal graphite. We assume that the anode plasma formation is dominated by adsorbed water and hydrocarbons.

IX. SUMMARY

An ion-beam diode has been fielded successfully on Mercury at ~4 MV and 10-12 Ohms. We obtain 20-25% ion efficiency with ion currents of 70-90 kA. These results are consistent with theory and with LSP calculations. Our results are insensitive to electron reflexing or anode surface condition. The forward-directed ion emission is dominated by the central region of the anode, and is improved by anode shaping. Further optimization in this area may be possible. The beam transports ballistically through a relatively small drift tube that enables good charge and current neutralization. We obtain over 10^{11} gammas/sr and can measure this signal cleanly, suppressing the spurious neutron flux and shielding the diode bremsstrahlung. We hope to improve on our measurement of the diode voltage by fielding a vacuum voltmeter [11] on Mercury in the future.

It is a pleasure to acknowledge the participation of Alan Hunt, Marcus Gagliardi, and Heather Seipel of the Idaho Accelerator Center of the Idaho State University in a successful collaboration that we hope to describe in a future publication.

It is also a pleasure to acknowledge a helpful collaboration with Tim Renk and Victor Harper-Slaboszewicz of Sandia National Laboratories. Joint experiments on Mercury are planned for the future.

X. REFERENCES

[1] R. J. Commisso, et al., "Application of TW-level pulsed power to the detection of fissile materials," these proceedings.
[2] B.J. Micklich, et al., "FIGARO: detecting nuclear materials using high-energy gamma-rays," NIM Phys Res A505, 1 (2003).
[3] R. J. Allen, et al., "Conversion of Mercury (a 2-TW Inductive Voltage Adder) to Positive Polarity," these proceedings.
[4] J. W. Schumer, et al., "Positive-polarity power flow in multiple-adder MITLs," these proceedings.
[5] LSP is a software product of ATK Mission Research, Albuquerque, NM87110.
[6] S.J. Stephanakis, et al., "Production of Intense Proton Beams in Pinched-Electron-Beam Diodes," Phys. Rev. Lett. 37, 1543 (1976).
[7] R.A. Meger and F.C. Young, "Pinched-Beam Ion Diode Scaling on the Aurora Pulser," J. Appl. Phys. 53, 8543 (1982).
[8] T. J. Renk, et al., "Generation of Ion Beams in Positive Polarity on HERMES III Operated in a Long-Pulse Mode," these proceedings.
[9] C.W. Mendel and S.E. Rosenthal, "Modeling Magnetically Insulated Devices Using Flow Impedance," Phys. Plasmas 2, 1332 (1995).
[10] Far West Technology, Goleta, CA, www.fwt.com.
[11] B. V. Weber, et al., "6 MV vacuum voltmeter development," these proceedings.